Structural Fluctuations and Excitation Transfer between Adenine and 2-Aminopurine in Single-Stranded Deoxytrinucleotides

John M. Jean*

Department of Biochemistry and Molecular Biophysics, Washington University School of Medicine, St. Louis, Missouri 63108

Brent P. Krueger*

Department of Chemistry, Hope College, Holland, Michigan 49422

Received: August 23, 2005; In Final Form: December 5, 2005

Steady-state fluorescence measurements on the deoxytrinucleotides $^{5'}$dTp2APpA$^{3'}$ and $^{5'}$dAp2APpA$^{3'}$ show a temperature-dependence and a viscosity-dependence for energy transfer that qualitatively differ from those seen in our previous study of charge transfer (CT) in these systems. Time-resolved anisotropy studies and molecular dynamics simulations are presented that provide a detailed characterization of the structural dynamics of these systems and how these fluctuations modulate the electronic interaction between 2AP and its neighbors. To gain quantitative insight into the interplay of conformational fluctuations and stacking-induced energy transfer, we present results from a new hybrid quantum-classical simulation method for computing the A → 2AP energy transfer rate that makes use of the full three-dimensional nature of the donor and acceptor transition densities. Analysis of the results shows that the standard transition dipole−transition dipole approximation for the Coulombic coupling substantially overestimates the transfer rate and that the nearest neighbor energy transfer from adenine to 2AP occurs on a much faster time scale than that for CT. This suggests that, unlike the CT dynamics where conformational "gating" plays a critical role, the large amplitude fluctuations that modulate the process are largely "frozen" out on the energy transfer time scale.

1. Introduction

The dynamics of nucleic acids are highly complex, with local fluctuations from the average structure occurring on time scales as short as picoseconds.[1−5] The fluorescent nucleobase 2-aminopurine (2AP) has proven to be a versatile probe of nucleic acid structure due to the sensitivity of its fluorescence properties to variations in the local environment.[6−22] Excitation into the 2AP S_1 ($\pi-\pi^*$) state ($\lambda_{max} \approx 305$ nm) leads to rapid charge transfer (CT) to neighboring nucleotides when 2AP is in a stacked conformation.[23−26] The magnitude of the resulting fluorescence quench is routinely used by experimentalists to describe the "extent" of stacking between 2AP and neighboring bases in nucleic acids and nucleic acid−protein complexes.

In addition to its useful CT properties, Nordlund and co-workers have demonstrated that neighboring purines are capable of transferring a bound excitation to 2AP within a DNA strand.[27−30] They observed stacking-induced electronic energy transfer (EET) bands in the adenine $\pi-\pi^*$ region (250−280 nm) of the fluorescence excitation spectra and 1−2 nm sequence-specific spectral shifts of the 2AP $\pi-\pi^*$ band in DNA oligomers in which 2AP is flanked by one or more adenines on either the 5′ or 3′ sides. Studies of 2AP-labeled adenosine pentamers suggest that an excitation may traverse two or more bases before being trapped by 2AP.[30] These results further extend the use of 2AP as a probe of DNA by providing an alternative observable, which may yield structural or dynamic information that is complementary to that provided by fluorescence quenching experiments. Indeed, measurements of the energy transfer band intensity have been used to probe the "melting" transition in duplex DNA,[27,28] the structure of ATAT and TATA sequences,[17] and the directional asymmetry of base stacking interactions in duplexes.[31]

Recent studies suggest that (sub)nanosecond conformational dynamics that alter base stacking act to "gate" the charge-transfer process in 2AP-labeled oligomers. Little effort, however, has been devoted to understanding the factors controlling energy transfer in these systems. The observation of efficient A → 2AP transfer in both single- and double-stranded oligomers suggests this process must be exceedingly rapid to compete effectively with the subpicosecond internal conversion process in adenine, although recent studies show that in dA•dT oligomers base stacking leads to "excimer" states with lifetimes ranging from 50 to 150 ps.[32]

The conventional starting point for calculating the rate of EET between a weakly coupled donor−acceptor pair is Förster theory,[33] which expresses the rate constant in terms of monomer spectral properties. Four critical assumptions are made in this approach: (1) the electronic and nuclear degrees of freedom are separable; (2) the donor−acceptor distance is sufficiently great compared to molecular dimensions that the full multipolar Coulombic interaction can be truncated to the transition dipole-transition dipole term; (3) the electronic coupling is time-independent (i.e., it does not couple to nuclear motions); and (4) the energetic fluctuations of the donor and acceptor states arising from nuclear motions are uncorrelated and much faster than the energy transfer time scale, which allows the effect of

* To whom correspondence should be addressed. E-mail: jjean@wanda.wustl.edu, kruegerb@hope.edu.

10.1021/jp054755+ CCC: $33.50
Published on Web 01/25/2006

these energetic fluctuations to be expressed in terms of the well-known spectral overlap integral.

The validity of each of these assumptions is questionable when considering excitation transfer in DNA or modified DNAs. DNA strands are structurally disordered, existing in solution as a broad continuum of stacked or partially stacked states, giving rise to a potentially wide range of electronic coupling values. The close proximity of bases, particularly in stacked conformations, requires consideration of the full multipolar nature of the coupling.[34] This close proximity also suggests that structural fluctuations may modulate the electronic interaction on a wide range of time scales.

In this paper, we present a combined experimental/theoretical study of thermal structural fluctuations and excitation transfer in the deoxytrinucleotides $^{5'}$dTp2APpA$^{3'}$ and $^{5'}$dAp2APpA$^{3'}$. These systems are highly flexible and, thus, serve as useful test systems for studying the photodynamics of 2AP in structurally disordered regions of nucleic acids, such as strand termini and loops. Circular dichroism spectra of these trinucleotides show evidence of extensive stacking, though they do not exhibit the canonical A- or B-form spectral signatures.[35] Molecular dynamics calculations place the barrier for the stacked → unstacked transition in DNA dimers and the ribonucleotide ApApA, for example, at 2−4 kcal/mol depending on sequence and which structural parameter is used as a metric for stacking.[36,37] In addition, positioning of the 2AP in the center of the trinucleotide allows us to focus solely on nearest-neighbor interactions, neglecting contributions from multiple hops from distant donors.

The paper is organized as follows: In Section 2, we describe the steady-state and time-resolved methods employed to characterize the dynamics of 2AP motion and A → 2AP EET efficiencies. In Section 3, we briefly review the Transition Density Cube (TDC) method of Krueger et al.,[38] which estimates the donor−acceptor Coulombic interaction from monomer transition densities. The method has as its limit an exact representation of the full multipolar expansion; thus, the resulting values for the Coulombic coupling are valid for the full range of donor−acceptor separations present in the ensemble. We also describe a new hybrid MD-TDC method for simulating the dynamic Coulombic interaction resulting from thermally induced structural fluctuations. Finally, we present a modified weak coupling model for computing the rate of energy transfer that maintains many of the features of the Förster theory but explicitly takes into account the three-dimensional nature of the donor and acceptor transition densities and properly averages over the structural fluctuations that modulate the Coulombic interaction. In Section 4, we present results from time-resolved fluorescence anisotropy experiments and molecular dynamics simulations that provide a detailed structural and dynamic characterization of the trinucleotides. Using the MD-TDC method, we determine the static and dynamic characteristics of the A-2AP Coulombic interactions and use these to compute average energy transfer rates. In Section 5, we summarize our findings and discuss the implications they have for 2AP as a site-specific probe of local DNA structure.

2. Experimental Methodology

Sample Preparation. The oligodeoxynucleotide trimers $^{5'}$dTp2APpA$^{3'}$, $^{5'}$dTp2APpT$^{3'}$, and $^{5'}$dAp2APpA$^{3'}$ were synthesized using phosphoramidites from Glen Research and purified by HPLC. Samples were prepared at concentrations of ∼5 μM (determined by absorption using 7200 M^{-1} cm^{-1} for the extinction coefficient of 2AP at 308 nm[11]) in a 10 mM sodium phosphate buffer (pH = 7) containing 100 mM NaCl. Absorption spectra were measured at T = 25 °C on a Shimadzu UV160U spectrophotometer.

Steady-State Fluorescence Measurements. Fluorescence excitation and emission spectra were measured using a PTI fluorometer equipped with a thermoregulated sample chamber. The spectra were corrected for the spectral response of the detector, and the fluorescence quantum yields (ϕ_{Trimer}) were determined using 2AP riboside (2APr) as a standard as described previously.[35] Energy transfer efficiencies (Φ) between donor (adenine) and acceptor (2AP), measured at excitation wavelength λ_{exc}, were determined using the measured absorption and excitation spectra according to the expression derived by Nordlund and co-workers[29]

$$\Phi = \frac{A_{2\mathrm{AP}}(\lambda_{\mathrm{exc}})}{A_{\mathrm{D}}(\lambda_{\mathrm{exc}})}\left[\frac{I_{\mathrm{Trimer}}(\lambda_{\mathrm{exc}})}{I_{2\mathrm{AP}}(\lambda_{\mathrm{exc}})}\left(\frac{\varphi_{2\mathrm{AP}}}{\varphi_{\mathrm{Trimer}}}\right) - 1\right] \qquad (2.1)$$

where $A_{2\mathrm{AP}}$ is the absorbance of the acceptor and A_{D} is the total absorbance of the donor bases. The latter is obtained from the absorbance of the trinucleotide after subtracting the contribution from 2AP. This assumes the absorbance of 2AP in this region is the same as that observed for 2APr. The 2AP fluorescence intensity, $I_{2\mathrm{AP}}(\lambda_{\mathrm{exc}})$, used in eq 2.1 is taken from measurements of the free 2APr; thus, the ratio of fluorescence intensities appearing in the brackets is multiplied by the ratio of quantum yields to take into account the intrinsic difference in fluorescence yields between the trinucleotide and the free nucleoside at a given temperature.

Time-Resolved Anisotropy Measurements. Picosecond fluorescence anisotropy decays were carried out using the time-correlated single photon counting instrument described in detail previously.[35] The laser system was a 76 MHz modelocked Ti:Sapphire oscillator (Coherent Mira 900F) pumped by a diode-pumped, frequency-doubled Nd:YVO_4 laser (Coherent Verdi-V10). The excitation wavelength (270 or 305 nm; vertically polarized) was obtained by frequency tripling the Ti:Sapphire fundamental. A short-wave pass filter was used to reject stray light and/or buffer fluorescence at wavelengths >400 nm, and a GG385 (Schott) high-pass filter was used to suppress the excitation and water Raman lines. The sample was contained in a thermostated 10 mm × 10 mm quartz cell. The full-width-half-maximum of the instrument response function was ∼150 ps, determined using the scattering from a dilute suspension of nondairy coffee creamer. Anisotropy decays were acquired by making separate measurements with equal acquisition times of the vertical and horizontal emission components. The vertical signal consisted of 2^{16} counts in the peak channel. Buffer fluorescence accounted for less than 2% of the total counts and was not subtracted from the sample decays prior to analysis. Anisotropies were constructed from the parallel ($I_{\parallel}(t)$) and perpendicular ($I_{\perp}(t)$) decays,

$$r(t) = \frac{I_{\parallel}(t) - GI_{\perp}(t)}{I_{\parallel}(t) + 2GI_{\perp}(t)} \qquad (2.2)$$

where G is a measure of the polarization bias of the detection system. The value of G was determined using tail matching of the parallel and perpendicular decay curves and was found to vary from 1.02 to 1.07. This approach is sufficient given that the depolarization time scale is faster than the average lifetime of 2AP in the trinucleotides.[35] The time-dependent anisotropy was fit using an iterative reconvolution procedure assuming a nonassociated biexponential decay of the form

$$r(t) = r(0)(\beta_1 e^{-t/\tau_1} + \beta_2 e^{-t/\tau_2}) \quad (2.3)$$

where β_i is the fractional limiting anisotropy of component i, τ_i is the corresponding rotational correlation time, and $r(0)$ the initial anisotropy.

3. Theoretical and Computational Methodology

Coulombic Coupling Calculations. The electronic coupling between a donor (D) and acceptor (A) comprises a Coulombic term and orbital overlap terms, which give rise to mixing of localized and CT states. The Coulombic term dominates for energy transfer involving allowed singlet states, as discussed by Scholes et al.[39] The orbital overlap terms are negligible for all structures except those in which the donor and acceptor are highly stacked; therefore, in this work, the overlap contributions to the total coupling are neglected. Here, we briefly review the transition density cube (TDC) method for computing the D−A Coulombic coupling, which can be expressed as the interaction between the transition densities, M^{eg}, of donor and acceptor:[40]

$$V^{Coul} = \int\int \frac{M_D^{eg}(r_D) M_A^{eg}(r_A)}{4\pi\epsilon_0 |r_D - r_A|} dr_D\, dr_A \quad (3.1)$$

where $M_i^{eg}(r_i)$ is the transition density for the g → e ($\pi-\pi^*$) transition.[41] In the TDC method, the transition densities are computed on a three-dimensional grid of finite-sized volume elements. The discretized form of the transition density is

$$M_i^{eg}(x, y, z) = V_\delta \int_x^{x+\delta x} \int_y^{y+\delta y} \int_z^{z+\delta z} \psi_i^g \psi_i^{e*}\, dx\, dy\, dz \quad (3.2)$$

where $V_\delta = \delta x \delta y \delta z$ is the volume element. Labeling the donor and acceptor grid elements j and j', respectively, the Coulombic coupling is given by

$$V^{Coul} = \sum_j \sum_{j'} \frac{M_D^{eg}(j) M_A^{eg}(j')}{4\pi\epsilon_0 |r_j - r_{j'}|} \quad (3.3)$$

The transition densities for the g → e ($S_0 \rightarrow S_1$) transitions of adenine and 2AP were computed using time-dependent density functional theory (TDDFT) at the B3LYP/6-311+G(d,p) level as implemented in the program QChem 2.0.[42] The ground-state geometries were obtained at the B3LYP/6-31G(p) level under C_s symmetry constraints. Each grid consisted of 48 000 elements (each with volume = 0.013 Å^3). Doubling the total number of points in the grid did not lead to significant differences in the values of the coupling.

When the TDCs are stored on disk, a limited number of significant figures are retained, leading to a nonzero total charge. If uncorrected, this charge would lead to a $1/r$ (monopole) interaction between the two molecules.[38] Thus, the total charge of each TDC is zeroed prior to calculating their interaction by subtracting a constant relative amount from each volume element.[43] This achieves the goal of nulling the charge of the TDC within the accuracy of the computer while altering the charge in each volume element only in the last significant digit that was stored on disk.

Transition dipoles (μ) for the lowest $\pi-\pi^*$ states of 2AP and adenine were determined by summing the contribution to the dipole moments of each grid element,

$$\mu_i^{eg} = \sum_j M_i^{eg}(j) r_{ij} \quad (3.4)$$

TABLE 1: Calculated (B3LYP/6-311G(d,p)) and Experimental $\pi-\pi^*$ Transition Moments

molecule	$\lvert\mu\rvert_{calc}$ (D)[a]	θ_{calc} (deg)	$\lvert\mu\rvert_{exp}$ (D)	θ_{exp} (deg)[b]	(μ_{exp}/μ_{calc})
2AP	2.90	+64	2.60[c]	+55	0.90
2APr	nd[d]	nd[d]	2.60[c]	−	−
Ade	2.92	+56	1.72[e]	+66 ± 7[f]	0.59
Ado	nd[d]	nd[d]	nd[d]	+65	−

[a] Units of Debye; 1 D = 1 × 10^{-18} esu = 3.34 × 10^{-30} C·m. [b] Transition dipole angle defined according to DeVoe−Tinoco convention (see Figure 4). [c] Based on an oscillator strength of 0.10 (ref 57). [d] nd = not determined. [e] Based on an oscillator strength of 0.05 (ref 57). [f] Result for 9-methyl-adenine (ref 58).

where r_{ij} is the vector from a specified origin of the ith monomer to the jth grid element of that monomer. The dipole−dipole coupling is given by

$$V^{d-d} = \frac{\vec{\mu}_D^{eg} \cdot \vec{\mu}_A^{eg}}{\mathbf{R}_{DA}^3} - \frac{3(\vec{\mu}_D^{eg} \cdot \vec{\mathbf{R}}_{DA})(\vec{\mu}_A^{eg} \cdot \vec{\mathbf{R}}_{DA})}{\mathbf{R}_{DA}^5} \quad (3.5)$$

where $\mathbf{R}_{DA}$ is the vector connecting the centers of the two dipoles.

The TDC method relies on accurate transition densities, which are usually obtained by ab initio or semiempirical methods. Because the magnitudes of calculated transition densities typically contain some error, we scale the charge in each volume element of the TDC by the ratio μ_{exp}/μ_{calc}, where μ_{exp} is the experimental value for the magnitude of the transition dipole. Note this procedure does not change the orientation or the nodal properties of the transition density with respect to the molecular frame. A good check for the accuracy of these properties is a comparison of the experimental and calculated transition dipole directions (cf. Table 1).

MD-TDC Simulations. Isothermal−isobaric (NPT) MD simulations of 5′dTp2APpA3′ and 5′dAp2APpA3′ were performed using the Cornell et al.[44] force field as implemented in AMBER 7,[45] which has been shown to accurately reproduce DNA structure both in crystal structures and solution structures.[46−48] In the last several years, the community of DNA simulation has converged on a relatively uniform protocol for accurate modeling of DNA dynamics and structure,[37,46,49−51] which is consistent with the protocol employed here. Simulations were performed using periodic boundary conditions with explicit TIP3P waters (∼2000 waters in a ∼(45 Å)^3 box). Sodium counterions were placed next to the phosphate groups for electrical neutrality, and additional sodium and chloride atoms were added to yield an effective salt concentration of ∼100 mM, identical to the experimental conditions. The particle mesh Ewald method was used for electrostatic interactions, and a 10 Å cutoff was used for evaluation of van der Waals interactions. Bonds involving hydrogen were fixed using the SHAKE algorithm to allow time steps of 2 fs. The system was equilibrated using 180 ps of NPT dynamics. Equilibration was deemed satisfactory by examination of the rmsd and total energy. Snapshots were saved every 1 ps. The total simulation time for each system was 10 ns.

The time-dependent Coulombic interaction between a donor adenine and 2AP was computed from the MD trajectories as follows: at each time point, each TDC was independently transformed onto the coordinates of the snapshot. Because the bond distances and bond angles within the rings fluctuate during the MD simulation, the transformed coordinates were obtained by fitting the positions of reference atoms (the C_4, C_5, and C_8 carbon atoms). This "rigid base" approximation neglects small deviations in the transition densities arising from changes in

ring geometry but has the advantage that the monomer transition densities need only be computed once. The coupling was then determined using eq 3.3 (using a value of 1.0 for ϵ_0), and the procedure was repeated for the next snapshot (every other snapshot was used giving a time step for the coupling of 2 ps).

Energy Transfer Model. In this section, we describe a theoretical model that goes beyond the Förster treatment in that (1) the dipole−dipole coupling is replaced by the full Coulombic interaction, and (2) the dynamic nature of this interaction arising from thermally induced structural fluctuations is explicitly treated. Like the Förster theory, our method is perturbative in the electronic coupling and retains the separation of electronic and nuclear degrees of freedom.

As noted above, recent time-resolved studies show that base stacking in polydA•dT oligomers leads to the formation of excimer states that are delocalized over more than one base.[32] The presence of such states in the systems discussed here would preclude the use of a weak-coupling approach for describing the energy transfer process. However, our use of a weak coupling is consistent with the experimental observations that the absorption spectra of the trimers closely resemble a superposition of monomer spectra (1−2 nm spectral shifts are observed, which are small compared to the bandwidths) and that the fluorescence spectra of the trinucleotides have band maxima and band shapes that are virtually identical to that of 2AP riboside (with no evidence for redder emission), suggesting emission from a localized 2AP state.

We also note that the broad absorption of adenine in the 250−280 nm region actually comprises two $\pi-\pi^*$ states with differing transition properties. According to our TDDFT calculations, the second lowest $^{5'}$dTp2APpA$^{3'}$ $\pi-\pi^*$ transition ($S_0 \rightarrow S_3$)[52] lies ∼2000 cm^{-1} higher than the $S_0 \rightarrow S_1$ transition with an oscillator strength approximately 70% that of the $S_0 \rightarrow S_1$ transition. Thus, due to inhomogeneous broadening of these transitions, it is likely that excitation results in a fraction of adenines excited into the higher state. We have calculated the TDC couplings between the 2AP $S_0 \rightarrow S_1$ and adenine $S_0 \rightarrow S_3$ transitions over a 1 ns portion of the $^{5'}$dTp2APpA$^{3'}$ trajectory during which the 2AP and adenine remained highly stacked. The average value of the interaction of the Ade-S_3 state with 2AP over this period was found to be ∼80% that of the Ade-S_1 state. In addition to the reduced Coulombic coupling, the Ade-S_3 state is expected to be a poor energy donor to 2AP because, though it is difficult to estimate quantitatively, the spectral overlap is significantly smaller than between the Ade-S_1 state and 2AP. Finally, the excitation wavelength used in this study (270 nm) is on the red edge of the adenine absorption spectrum, which should result primarily in direct excitation of the S_1 state. Thus, in our model, we assume only the lowest $\pi-\pi^*$ state of adenine is active in energy transfer.

In the weak-coupling limit, the expression for the rate of energy transfer is

$$k = \frac{2\pi}{\hbar}|V|^2\,\rho(q_D)\rho(q_A) \tag{3.6}$$

where V represents the donor (Ade)−acceptor (2AP) Coulombic interaction and $\rho(q_D)$ and $\rho(q_A)$ are the Franck−Condon envelopes for the donor and acceptor transitions, respectively. q_D and q_A represent the mutually exclusive sets of vibrational modes that couple energetically to the monomer states and are thus responsible for the spectral line shapes of the monomer $\pi-\pi^*$ transitions. For the nucleobases, these FC-active modes comprise intramolecular motions as well as dipolar fluctuations of the solvent. As in Förster's treatment, we assume these modes relax on a time scale faster than the inverse of the transfer rate and thus are assumed to be thermally averaged. This yields the well-known result for the energy transfer rate in terms of the spectral overlap integral, J_{DA}.

$$k = \frac{2\pi}{\hbar}|V|^2 J_{DA} \tag{3.7}$$

where

$$J_{DA} = \int N_D \frac{f_D(\nu)}{\nu^3} N_A \frac{\epsilon_A(\nu)}{\nu} d\nu \tag{3.8}$$

and

$$\int N_D \frac{f_D(\nu)}{\nu^3} d\nu = \int N_A \frac{\epsilon_A(\nu)}{\nu} d\nu = 1$$

on the wavenumber scale. $f_D(\nu)$ and $\epsilon_A(\nu)$ are the experimentally determined donor fluorescence intensity and acceptor molar extinction coefficient, respectively.

The role of structural dynamics in DNA-mediated charge transfer is becoming increasingly appreciated.[5,35,53−55] Troisi et al.[55] have presented a theoretical model for calculating the average rate of charge transfer between nucleobases separated by a flexible "bridging sequence", which clearly exposes the contributions of both static and dynamic disorder in the interbase electronic couplings. To incorporate structural heterogeneity into a Förster-like rate theory, we follow their example and posit a second set of modes that couple to the Coulombic interaction. Motion along these coordinates alters the relative geometry of the donor and acceptor bases and would include large-amplitude motions, such as sugar−phosphate backbone torsions and glycosidic bond rotations. Inclusion of the "structural" modes in the model leads to a time-dependent Coulombic interaction, which can be incorporated into the rate expression,

$$k = \frac{2\pi}{\hbar}|V(Q(t))|^2\,J_{DA} \equiv \frac{2\pi}{\hbar}|V(t)|^2\,J_{DA} \tag{3.9}$$

The structural modes (Q) are assumed to be low frequency and are treated via classical molecular dynamics simulations. In what follows, we will assume that these two sets of modes (q, Q) are mutually exclusive.

While the FC modes are assumed to relax faster than the transfer time scale, no assumptions are made regarding the time scale(s) of structural modes. If these motions were also fast compared to the energy transfer time scale, we could replace $V(t)$ in eq 3.9 with its thermal average. In the absence of such a separation of time scales, the geometry-dependent energy transfer rate will lead to complex donor-decay kinetics. In such a case, the relation between the transfer rate and the transfer efficiency becomes ambiguous. We can calculate an efficiency based on an average rate constant for energy transfer by writing the dynamic coupling as

$$V(t) = \langle V\rangle + \delta V(t) \tag{3.10}$$

where $\langle V\rangle$ is the time-averaged value defined such that $\langle \delta V(t)\rangle = 0$, where $\langle\cdots\rangle$ represents an average over the thermal ensemble. As demonstrated by Troisi et al., this allows the definition of a time-averaged rate constant in terms of the spectral density function, $\Gamma(E)$, which contains all the information on the off-diagonal disorder,[55]

$$\Gamma(E) = \frac{2\pi}{\hbar}\langle V^2\rangle\delta(E) + \frac{1}{\hbar^2}\int_{-\infty}^{+\infty}\langle\delta V(t)\delta V(0)\rangle\, e^{-(i/\hbar)Et}\, dt \quad (3.11)$$

These authors developed a series expansion of the rate constant that clearly exposes the contributions to the average rate arising from static and dynamic disorder in the electronic coupling. For a coupling time-correlation function that decays exponentially with a time constant τ_c, the rate constant to second order in the coupling is given by

$$k = \frac{2\pi}{\hbar}\langle V^2\rangle J_{DA} + \frac{\pi\hbar}{\tau_c^2}\langle\delta V^2\rangle\left(\frac{d^2 J_{DA}(\Delta E)}{d\Delta E^2}\right)_{\Delta E=\Delta E_0} \quad (3.12)$$

where ΔE is the energy difference between the electronic origins of the donor and acceptor transitions (in our model taken to be the difference in the spectral maxima) and ΔE_0 is the actual energy difference (obtained from the experimental spectra). The relative importance of the dynamic correction term is thus determined not only by the magnitude of the fluctuating coupling (compared to the average value), but also by the fluctuation time scale. In their application of eq 3.12 to DNA-mediated charge transfer, Troisi et al. modeled the fluctuating coupling as a Gaussian random process with $\langle V\rangle^2/\langle V^2\rangle$ and τ_c as parameters. Here, we compute these values from our MD-TDC simulations of $V(t)$.

4. Results and Discussion

Trinucleotide Spectral Properties. The ultraviolet absorption spectra of 2AP riboside (2APr) and the trinucleotides $^{5'}$dTp2APpA$^{3'}$ and $^{5'}$dAp2APpA$^{3'}$ at $T = 25$ °C are shown in Figure 1a. The 2AP $\pi-\pi^*$ bands occur at 305 and 245 nm. The strong absorption in the 250−280 nm region is from the $\pi-\pi^*$ transitions of the flanking bases. The spectra closely resemble the sum of the monomer base spectra, though there is theoretical evidence that mixing of the ground state HOMOs alters the oscillator strength of the 2AP transition in highly stacked geometries.[25]

Fluorescence excitation spectra of $^{5'}$dTp2APpA$^{3'}$, $^{5'}$dAp2APpA$^{3'}$, and $^{5'}$dTp2APpT$^{3'}$ at $T = 25$ °C are shown in Figure 1b. The latter compound is used here as a control. The energy transfer band in the adenine-containing systems is clearly visible in the 260−280 nm region. The lack of this band in $^{5'}$dTp2APpT$^{3'}$ demonstrates that in the asymmetric trinucleotide $^{5'}$dTp2APpA$^{3'}$, the peak at 270 nm reflects the transfer of an excitation to the central 2AP from adenine. Also evident in both the absorption and excitation spectra of the adenine-containing systems is the 1−2 nm red-shift in the 2AP band arising from stacking interactions, as has been discussed by Davis et al.[30] In Figure 2, normalized difference excitation spectra (trinucleotide minus 2APr) for $^{5'}$dAp2APpA$^{3'}$ as a function of temperature are plotted. The plot shows a strong correlation between the magnitude of the 2AP band shift and the intensity of the energy transfer band, demonstrating the influence of thermally induced changes in the distribution of stacked states on the transfer efficiency. This behavior is in marked contrast with the (nearly) temperature-independent charge-transfer kinetics seen in our earlier study of these systems.[35]

Energy Transfer Efficiencies. The energy transfer efficiency can be computed from the measured absorption and emission spectra of 2APr and the trinucleotides using eq 2.1. Because the total absorption of the two flanking bases appears in the denominator, this yields the transfer efficiency averaged over all bases absorbing at the excitation wavelength (270 nm), i.e., in this case, both flanking bases. Thus for $^{5'}$dAp2APpA$^{3'}$, it is not possible to determine the relative efficiencies for transfer from the 5′ and 3′ sides. In this case, we assume the 5′ and 3′ adenines make equal contributions to the absorption spectrum and report the mean transfer efficiency per donor. For $^{5'}$dTp2APpA$^{3'}$, the computed transfer efficiency contains the null contribution from the thymine; thus, to arrive at an efficiency for the $^{3'}$A → 2AP transfer in this system, we subtract the contribution of the thymine to the total absorbance in eq 2.1 by assuming the extinction coefficient at 270 nm for thymine in the context of the trinucleotide is equal to that of thymidine in solution. The efficiencies for $^{5'}$dTp2APpA$^{3'}$ and $^{5'}$dAp2APpA$^{3'}$ are shown over the temperature range $T = 10-60$ °C in Figure 3. Two features of the energy transfer process are readily apparent. First, the average efficiency per adenine in $^{5'}$dAp2APpA$^{3'}$ is greater than the efficiency of transfer from the 3′ adenine in $^{5'}$dTp2APpA$^{3'}$. Second, the rate of energy

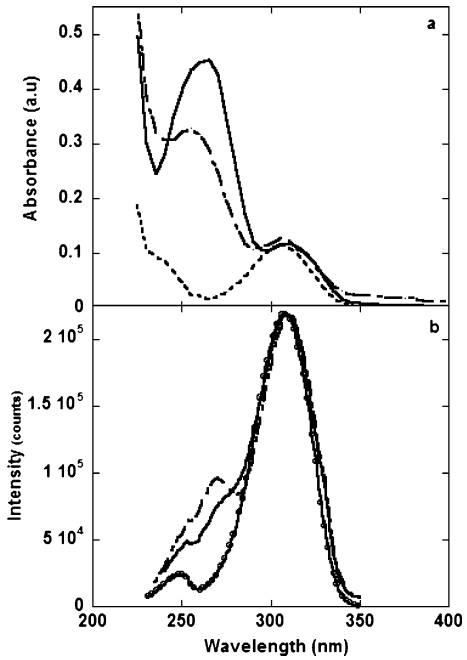

Figure 1. (a) Absorption spectra of $^{5'}$dTp2APpA$^{3'}$ (solid), $^{5'}$dAp2APpA$^{3'}$ (dashed), and 2-aminopurine riboside (2APr) (dotted) at $T = 25$ °C and pH = 7 in 10 mM sodium phosphate/100 mM NaCl (pH = 7). Concentrations were 5 μM (determined using 7200 M^{-1} cm^{-1} for the extinction coefficient of 2APr at 305 nm). (b) Fluorescence excitation spectra of $^{5'}$dTp2APpA$^{3'}$(solid), $^{5'}$dAp2APpA$^{3'}$(dashed), and $^{5'}$dTp2APpT$^{3'}$(solid line circles) under the same solution conditions shown in (a). The excitation spectrum of 2APr (not shown) is identical to that of $^{5'}$dTp2APpT$^{3'}$. Emission wavelength = 368 nm.

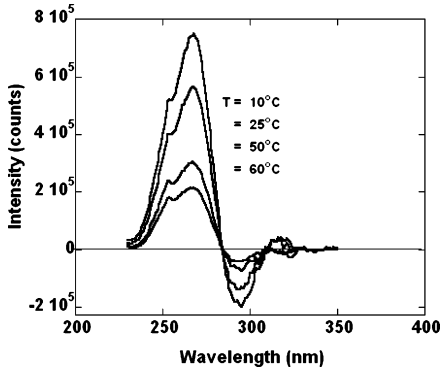

Figure 2. (a) Difference excitation spectra ($I_{trinucleotide}$-I_{2APr}) for $^{5'}$dAp2APpA$^{3'}$ at the indicated temperatures. The two excitation spectra have been normalized to the same 2AP fluorescence quantum yield as described in ref 29.

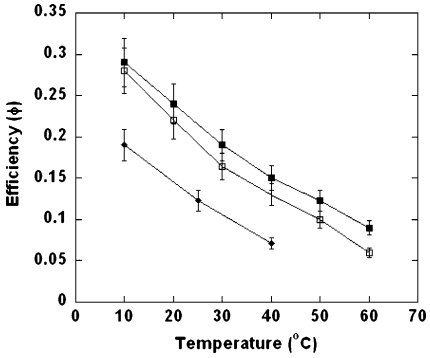

Figure 3. Energy transfer efficiencies as a function of temperature: (■) $^{5'}$dAp2APpA$^{3'}$, 0% glycerol; (□) $^{5'}$dAp2APpA$^{3'}$, 60% glycerol; (◆) $^{5'}$dTp2APpA$^{3'}$, 0% glycerol.

transfer is relatively insensitive to changes in viscosity. The transfer efficiency in $^{5'}$dAp2APpA$^{3'}$ decreases less than ~10% at a given temperature upon addition of glycerol (60%) to the buffer, which corresponds to a 7−9-fold increase in the viscosity over the temperature range studied.

Not surprisingly, attempts to time-resolve the rising edge of the fluorescence from the acceptor 2AP following excitation at 270 nm were unsuccessful due to the limited resolution of our time-correlated single photon counting instrument. We can, however, estimate the rate constant for energy transfer, k_t, from the measured efficiency using the relation

$$\phi = \frac{k_t}{k_t + k_d} \tag{4.1}$$

where k_d is the donor decay rate in the absence of the acceptor, i.e., the inverse of the adenine $\pi-\pi^*$ lifetime. The lifetime of adenosine in solution is 290 fs, as reported recently by Pecourt et al.[56] If we assume the lifetime of the donor adenine is independent of structural context, then at T = 25 °C, the estimated A → 2AP transfer rate in $^{5'}$dTp2APpA$^{3'}$ is $k_t \approx$ (1.7 ps)$^{-1}$ and in $^{5'}$dAp2APpA$^{3'}$ is $k_t \approx$ (1.0 ps)$^{-1}$. We note that using the adenosine decay rate eq 4.1 is only valid if the donor state in the presence of the acceptor remains localized on the adenosine, which follows from the weak-coupling assumption.

As noted earlier, the dynamics of charge transfer in these systems reflects the competition between low-barrier stacking−unstacking processes that modulate the π-orbital overlap and the overlap-dependent electron tunneling. The temperature dependence and viscosity dependence of the energy transfer efficiency suggest that, in this case, structural fluctuations and Coulombic interactions conspire differently than in the case of charge transfer. Further insight into the interplay between structural fluctuations and electronic interactions in these systems can be gained from detailed characterization of the local dynamics of 2AP in these structures and the resulting fluctuations in the nearest neighbor interactions.

π*−*π* **Transition Dipoles and Transition Densities.** Implementation of the MD-TDC method requires accurate transition densities for the lowest energy $\pi-\pi^*$ transitions in 2AP and adenine. From the transition densities we can extract transition dipole magnitudes and directions, which will be used both to assess the validity of the dipole−dipole approximation and to model our time-resolved fluorescence anisotropy results. Figure 4a shows the calculated transition densities for the lowest $\pi-\pi^*$ transitions of adenine and 2AP. Figure 4b shows the corresponding transition dipoles computed from these densities using eq 3.4 along with those obtained from recent linear dichroism experiments.[57,58] These are summarized in Table 1. For 2AP,

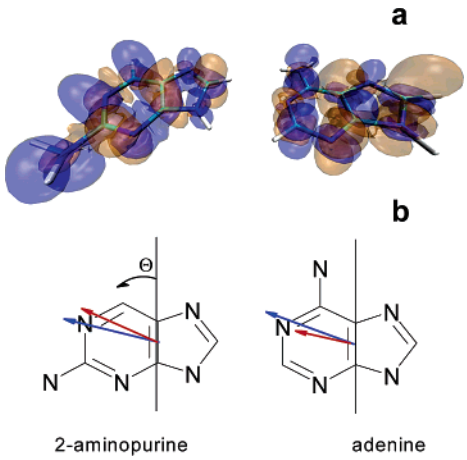

Figure 4. (a) Transition densities of 2-aminopurine and adenine calculated using TDDFT (B3LYP/6-311+G(d,p)). (b) Transition dipole directions and relative magnitudes obtained from eq 3.4 (blue); experimental determinations (red) (2AP − ref 57; adenine − ref 58). ϕ denotes the positive direction for the transition dipole orientation.

the calculated transition dipole magnitude and direction are in good agreement with results from the absorption and linear dichroism studies of 2AP oriented in a PVA film.[57] The presence of the N7 tautomer as well as perturbations arising from crystal packing forces has rendered accurate determination of the transition dipole properties for adenine difficult;[59] hence, experimental results for adenine vary considerably, and most experimental studies suggest a much smaller angle for the transition dipole than predicted from our TDDFT results. Substitution at the N9 position (e.g., by ribose in DNA) precludes the presence multiple tautomers and has been shown to only slightly perturb the direction of the transition dipole.[58] Given these facts, we compare our TDDFT result for adenine to the recent experimental values of Holmen et al. for 9-methyladenine (9MA) and adenosine (Ado),[58] which provide the best experimental comparison to adenine in the context of DNA. As can be seen from Figure 4b and Table 1, the directions agree quite well (~10°); however, TDDFT predicts a magnitude nearly 70% larger than the magnitude obtained from the experimental oscillator strength. The good agreement between calculated and experimental dipole directions and the scaling of our calculated transition densities to the experimental dipole values leads us to conclude that the calculated transition densities (and resulting Coulombic coupling strengths) are obtained quite reasonably.

Depolarization Dynamics of 2-Aminopurine. Time-resolved fluorescence anisotropy experiments probe orientational fluctuations of the 2AP transition dipole and thus provide a direct measure of the time scale of 2AP motion. The time-resolved signal is given by[60]

$$r(t) = \frac{2}{5}\langle P_2[\hat{\mu}_A(0)\cdot\hat{\mu}_E(t)]\rangle \tag{4.2}$$

where $P_2(x)$ is the second-order Legendre polynomial and $\hat{\mu}_A$ and $\hat{\mu}_E$ are the unit transition dipole vectors for the absorbing and emitting states, respectively. For direct excitation of 2AP, the absorbing and emitting dipoles are assumed to be parallel in the molecular frame (i.e. $\mu_A = \mu_E = \mu_{2AP}$), and the initial anisotropy should be close to the maximum value of 0.40. For excitation into the adenine region of the spectrum, energy transfer between the photoexcited adenine and 2AP results in an additional depolarization mechanism because $\mu_A \neq \mu_E$. If the A → 2AP excitation transfer process is much faster than the time scale of 2AP motion, then the time-resolved 2AP signal

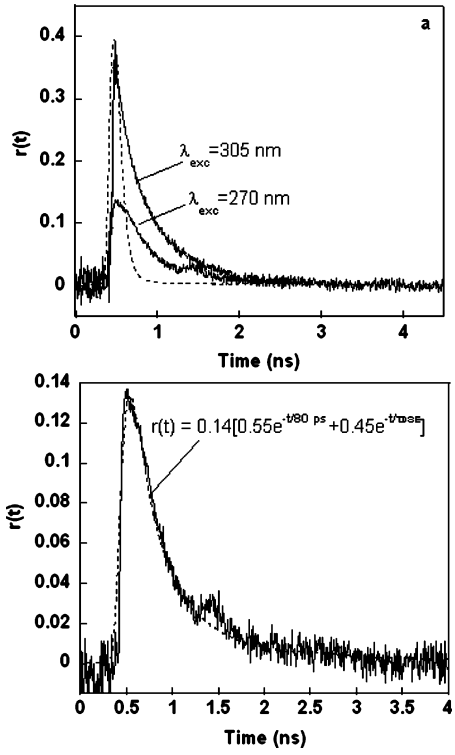

Figure 5. (a) Time-resolved fluorescence anisotropy of $^{5'}$dTp2APpA$^{3'}$ at $T = 25$ °C (0% glycerol) at the indicated wavelengths. The dotted line is the instrument response function. (b) Two-exponential fit of the time-resolved fluorescence anisotropy decay at $\lambda_{exc} = 270$ nm.

provides a direct measure of the dynamics of the 2AP ring, whereas the value of $r^{eff}(0)$ reflects the equilibrium distribution of the relative orientations of the adenine and 2AP rings. In this case, we can rewrite eq 4.2 as

$$r(t) = r^{eff}(0)\langle P_2[\hat{\mu}_{2AP}(0)\cdot\hat{\mu}_{2AP}(t)]\rangle$$
$$\text{with } r^{eff}(0) = \langle P_2[\hat{\mu}_{ade}(0)\cdot\hat{\mu}_{2AP}(0)]\rangle = \frac{2}{5}\langle P_2[\cos\theta(0)]\rangle \le 0.40 \quad (4.3)$$

where $\theta(0)$ is the angle between the adenine and 2AP transition dipoles at $t = 0$. We have carried out anisotropy measurements on $^{5'}$dTp2APpA$^{3'}$ using both direct excitation of 2AP and excitation in the adenine region of the spectrum at 270 nm. The experimental decays obtained at $T = 25$ °C using 305 and 270 nm excitations are shown in Figure 5a. The 305 nm decay curve was fit adequately by the double exponential function eq 2.3 to give $r(t) = 0.35[0.38\ \exp(-t/80\ \text{ps}) + 0.62\ \exp(-t/490\ \text{ps})]$ ($\chi^2 = 1.12$). The difference between our experimental value for $r(0)$ of 0.36 and the theoretical maximum of 0.40 most likely reflects small amplitude fluctuations of the 2AP ring and/or solvent dynamics on time scales faster than our temporal resolution.

The above result shows that the initial polarization in the sample following direct excitation of 2AP is substantially depolarized by 100−200 ps. A similar decay time is seen for the 270 nm decay curve, which is shown in Figure 5b. In this case, achieving an adequate fit to a double exponential decay was problematic, possibly due to the very low fluorescence signal at this excitation wavelength. Despite this difficulty, it is clear that the depolarization time scale is similar at the two excitation wavelengths, as expected.

It is interesting to compare this time scale with that predicted if the trinucleotide behaved like a rigid, stacked system. In this case, the only depolarization mechanism would be rotational diffusion. We can estimate the rotational correlation time for the rigid trinucleotide (assuming it is spherical) from the Debye−Stokes−Einstein equation ($\tau_{rot} = \eta V/kBT$, where η is the viscosity and V is the hydrodynamic volume). For a hydrated sphere with an anhydrous volume of 812 Å^3 (computed from a space-filling model for B-form dTp2APpA) and a typical hydration volume of 0.5 cm$^3\cdot$g^{-1}, the rotational correlation time at 25 °C is ∼400 ps in 0% glycerol (∼1 cP). This result is similar in value to the longer component seen in the anisotropy decays. The presence of a short component with nearly 50% amplitude strongly suggests that although the system is highly stacked, there is considerable local motion of the 2AP.

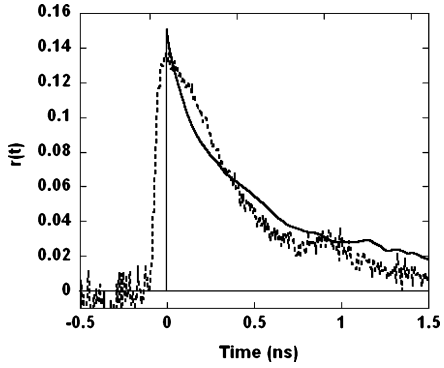

Figure 6. Short time anisotropy ($\lambda_{exc} = 270$ nm) of $^{5'}$dTp2APpA$^{3'}$: (solid) experimental; (dashed) molecular dynamics simulation.

The main effect of excitation in the adenine region on the observed anisotropy is a dramatic reduction in the value of $r(0)$ from 0.36 to 0.13. As noted above, this is a direct result of ultrafast A → 2AP energy transfer and provides insight into the relative orientation of these bases in the equilibrium ensemble. The time-resolved anisotropy of $^{5'}$dTp2APpA$^{3'}$ at $\lambda_{exc} = 270$ nm can be modeled using the molecular dynamics trajectory. This is done in two separate steps using snapshots taken at 1 ps intervals and writing eqs 4.3 as

$$r^{eff}(0) = \langle P_2[\hat{\mu}_{ade}(0)\cdot\hat{\mu}_{2AP}(0)]\rangle \approx \frac{1}{N}\sum_{n=1}^{N} P_2[\hat{\mu}_{ade}(t_n)\cdot\hat{\mu}_{2AP}(t_n)]$$
$$r(t_m) = r^{eff}(0)\langle P_2[\hat{\mu}_{2AP}(0+)\cdot\hat{\mu}_{2AP}(t_m)]\rangle \approx \frac{1}{N-m}\sum_{n=1}^{N-m} P_2[\hat{\mu}_{ade}(t_n)\cdot\hat{\mu}_{2AP}(t_{n+m})] \quad (4.4)$$

where N (= 10 000) is the number of snapshots. The simulated anisotropy for $^{5'}$dTp2APpA$^{3'}$ at $T = 25$ °C is compared with the experimental result over the first 1.5 ns of decay in Figure 6. For times longer than this, the sampling statistics become increasingly poor. Overall rotation of the trinucleotide during the simulation was not removed before the calculation; thus, the computed $r(t)$ contains contributions from both the local fluctuations of the 2AP ring and global tumbling of the trinucleotide; however, the latter is poorly sampled on the simulation time scale. The computed decay curve (which is not convoluted with the instrument response) shows reasonable agreement at short times, suggesting the dynamical time scales present in the simulation are similar to those occurring in solution. In addition, the experimental and calculated values for $r^{eff}(0)$ are in excellent agreement, suggesting that the relative geometries of 2AP and adenine sampled during the simulation are representative of the ensemble of structures existing in solution.

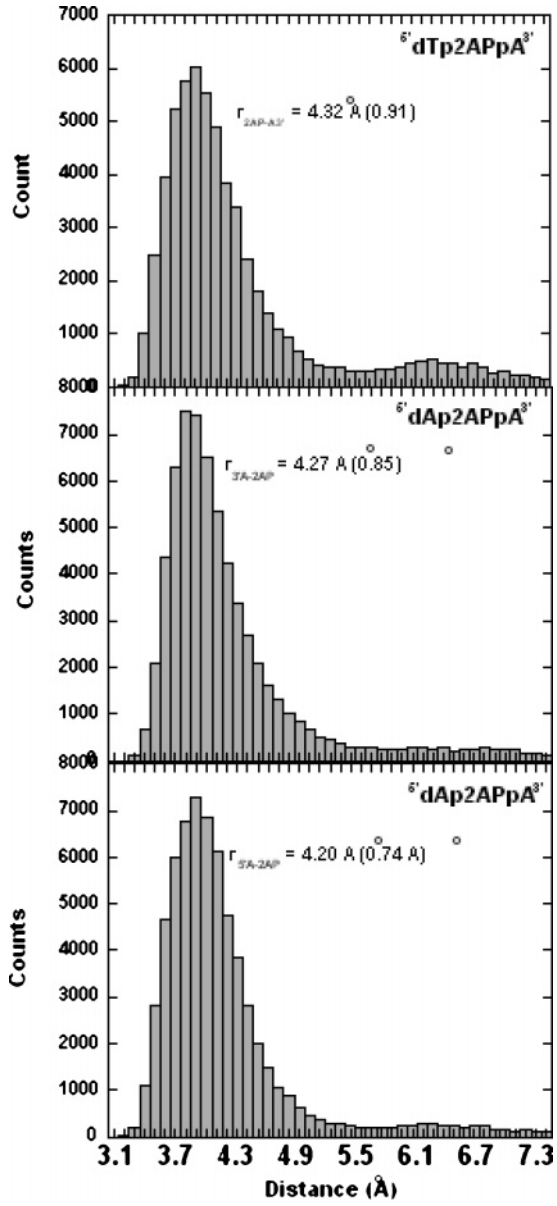

Figure 7. A-2AP center-of-mass distance distributions for $^{5'}$dTp2APpA$^{3'}$ (2AP-A$^{3'}$), $^{5'}$dAp2APpA$^{3'}$(2AP-A$^{3'}$), and $^{5'}$dAp2APpA$^{3'}$ ($^{5'}$A-2AP). Total simulation time for each trinucleotide was 10 ns; distances calculated at 0.10 ps intervals.

Stacking−Unstacking Dynamics. The time-resolved fluorescence anisotropy results provide the time scale for 2AP motion in the context of the trinucleotides but do not directly address the important question of the time scales associated with fluctuations of the donor−acceptor geometries. The MD simulation results also allow us to characterize these fluctuations. Figure 7 shows plots of the distribution of the $^{5'}$A-2AP center-of-mass distances in $^{5'}$dAp2APpA$^{3'}$ and the 2AP-A$^{3'}$ distances in both $^{5'}$dTp2APpA$^{3'}$ and $^{5'}$dAp2APpA$^{3'}$, generated using 100 000 snapshots taken at 0.1 ps intervals. For an A-2AP stacked in B-form geometry, the center of mass distance is ∼3.9 Å. Comparison of the distributions in the top two panels shows that the 3′ adenine stacking−unstacking energetics is influenced to some extent by the identity of the 5′ base**.** In the case of $^{5'}$dAp2APpA$^{3'}$, the mean and widths of the two A-2AP distance distributions suggests that the underlying stacking−unstacking energetics for the 5′ and 3′ adenines are similar, at least in the region of the potential surface near the minimum. If we arbitrarily assign a distance of $r \geq 5.5$ Å as corresponding to an unstacked conformation, we see that both the 5′ and 3′ adenines spend greater than 90% of their time in a stacked state. Also, the distribution in the unstacked region is relatively flat, particularly for $^{5'}$dAp2APpA$^{3'}$, reflecting the absence of a minimum in this region of the potential surface.

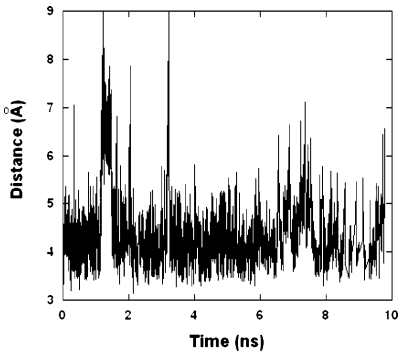

Figure 8. 2AP-A$^{3'}$ center-of-mass distance as a function of time.

Temporal fluctuations in the 2AP-A distance in $^{5'}$dTp2APpA$^{3'}$ are shown in Figure 8. Numerous excursions of the 3′ adenine into unstacked conformations occur over this time scale. Similar results are seen for both A-2AP distances in $^{5'}$dTp2APpA$^{3'}$ (data not shown). The distribution of observed residence times in an unstacked state is quite broad and asymmetric, with most of the unstacked conformations surviving only a few tens of ps but some as long as several hundred ps. This picture of a predominately stacked but highly dynamic structure is in agreement with our earlier interpretation of the absence of a long-lived 2AP component in the fluorescence decay in these systems.[35]

Dynamic Coulombic Coupling. The MD-TDC method allows us to assess the range of validity of the dipole−dipole approximation and to investigate the effect of structural fluctuations on the magnitude of the Coulombic interactions. A 2 ns portion of the dipole−dipole and TDC trajectories for $^{5'}$dTp2APpA$^{3'}$ is shown in Figure 9a. In this panel, the squares of the couplings are plotted to emphasize the effect of structural fluctuations on the instantaneous value for the energy transfer rate. This section of the trajectory clearly illustrates the heterogeneity in both the Coulombic coupling and the lifetime of unstacked conformations. In regions where the 3′A is clearly in an unstacked conformation (e.g., ∼1.2−1.5 ns), agreement between the full Coulombic coupling and dipole−dipole approximation is reasonable, as expected. In stacked or partially stacked conformations, the dipole−dipole result nearly always overestimates the true coupling strength. The fraction of structures for which the dipole−dipole approximation breaks down can be seen from Figure 9b, which shows a plot of the TDC results vs the dipole−dipole coupling. Clearly, both approaches predict that the value of the Coulombic coupling is highly sensitive to donor−acceptor geometry; however, at distances where the dipole−dipole approach fails, the dipole−dipole result also overestimates the sensitivity to conformational changes.

The above results demonstrate that the Coulombic coupling in these trinucleotides is highly dynamic; however, a critical property to consider is the fluctuation time scale, which allows us to determine the dynamic contribution to the energy transfer rate. This is done using snapshots from our md simulation taken at 2 ps intervals and writing the correlation function as

$$\langle \delta V(t_m) \cdot \delta V(0) \rangle = \frac{1}{N-m} \sum_{n=1}^{N-m} [\delta V(t_{n+m}) \delta V(t_n)] \quad (4.5)$$

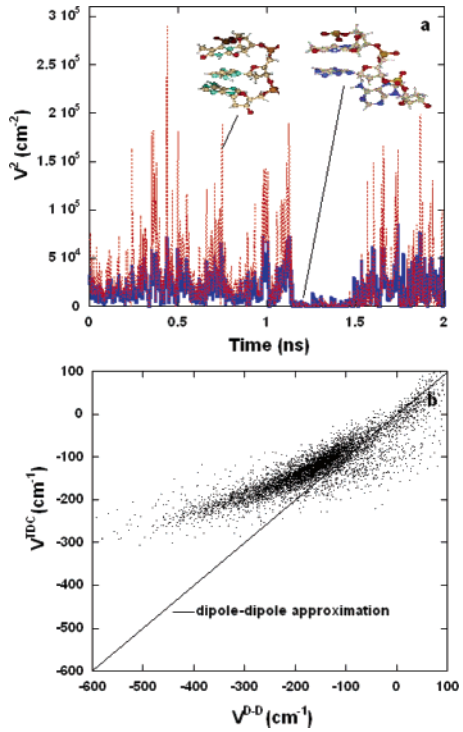

Figure 9. (a) Time-dependence of the full Coulombic coupling (V^{TDC}; solid blue line) and the dipole−dipole coupling (V^{DD}; dashed red line) for $^{5'}$dTp2APpA$^{3'}$ calculated from the MD-TDC method. The time range corresponds to the first 2 ns of the 2AP-A$^{3'}$ trajectory shown in Figure 8. (b) Comparison of the full Coulombic and dipole−dipole couplings for 2AP-A$^{3'}$.

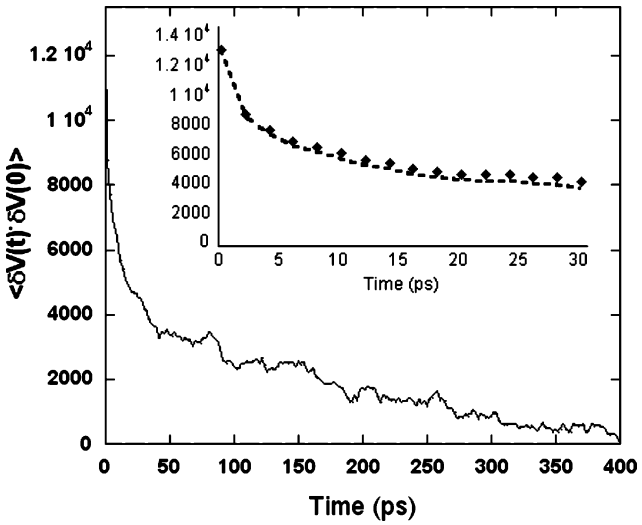

Figure 10. Time-correlation function for the fluctuation of the A-2AP$^{3'}$ Coulombic coupling, $\langle \delta V(t) \cdot \delta V(0) \rangle$, for $^{5'}$dTp2APpA$^{3'}$ calculated at 2 ps intervals from the MD-TDC method. Inset: comparison of the short time decay (dashed) and the double exponential decay function $F(t) = 0.66 \exp(-t/6 \text{ ps}) + 0.34 \exp(-t/250 \text{ ps})$.

Figure 10 shows this function for the A-2AP Coulombic coupling in $^{5'}$dTp2APpA$^{3'}$. The short time behavior (inset) can be approximated by a two exponential function consisting of 6 and ~250 ps components (see caption).

As noted earlier, the energy transfer efficiencies suggest that in the trinucleotides, the 5′ adenine is the more efficient donor. Using the center-of-mass distance as a metric for stacking, it was shown in Figure 7 that the distribution of $^{5'}$A-2AP and 2AP-A$^{3'}$ stacked states are similar. This is clearly not the case for the corresponding distributions of coupling strengths, as shown in Figure 11. The mean value for the TDC coupling is

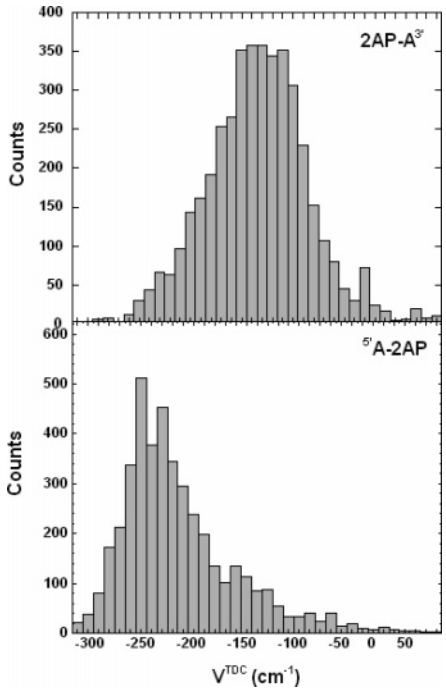

Figure 11. Distributions of the 2AP-A$^{3'}$ and $^{5'}$A-2AP Coulombic couplings for $^{5'}$dAp2APpA$^{3'}$ calculated from the MD-TDC method.

substantially greater for $^{5'}$A-2AP. Clearly, the magnitude of the Coulombic interaction provides a useful electronic metric for stacking as compared to conventional structural metrics and, in the case of $^{5'}$dAp2APpA$^{3'}$, yields results for the extent of stacking that differ from those predicted by typical structural metrics. The lack of a clear peak near $V = 0$ in these distributions is a result of the wide range of orientations (and hence coupling values) that are sampled when the donor−acceptor distance is large.

Energy Transfer Rates. From the statistics of the fluctuating Coulombic coupling, we can compute ensemble-averaged rates of energy transfer via eq 3.12. In doing so, we consider only the shorter (6 ps) component of the computed coupling correlation function. This allows us to estimate the upper limit of the dynamic contribution to the rate. We still need, however, to consider the overlap of the density-weighted Franck−Condon factors, J_{DA}, which reflects the contribution to the rate from intramolecular vibrations and solvent motions. As in the Förster theory, we compute J_{DA} from the experimental spectra using eq 3.8. The normalized adenosine fluorescence and 2APr absorption spectra are shown in Figure 12. The spectral overlap integral and its second derivative were determined numerically giving $\rho = 8.69 \times 10^{-5}$ cm and $(d^2\rho/d\Delta E^2)_{\Delta E=\Delta E_0} = -6.2 \times 10^{-15}$ cm^3.

In their application of eq 3.11 to DNA-mediated charge transfer, Troisi et al. modeled the fluctuating coupling, $\delta V(t)$, as a Gaussian random process with $\langle V \rangle^2/\langle V^2 \rangle$ and τ_c as parameters.[55] Here, we compute these values from our MD-TDC simulations of $V(t)$. The various parameters that go into eq 3.12 as well as the resulting inverse rate constants (i.e., energy transfer times) computed using both the dipole−dipole approximation and the TDC method are shown in Table 2. The dipole−dipole approximation is reasonable only for those structures that are unstacked and predicts an ensemble-averaged transfer rate that is faster by a factor of 2 from that predicted by the TDC method. The MD-TDC method, though considerably superior to the standard Förster calculation, still overestimates the transfer rate derived from the experimental efficien-

TABLE 2: Rate Parameters for A → 2AP Energy Transfer

donor acceptor	$\langle V^2\rangle$ (cm^{-2})	$\langle V^2\rangle/\langle V^2\rangle$	τ_c (ps)[a]	k_d/k_s	$k_{TDC(ps)}^{-1}$	$k_{DD(ps)}^{-1}$	$k_{expt(ps)}^{-1}$[b]
$^{5'}$dTp**2APpA**$^{3'}$	17,640	0. 74	6	$\sim10^{-9}$	0.57	0.27	1.8
$^{5'}$dAp**2APpA**$^{3'}$	20,414	0.86	5	$\sim10^{-9}$	0.48	0.23	−
					{0.32}[c]	{0.14}[c]	{0.93}[b]
$^{5'}$**dAp2AP**pA$^{3'}$	44,735	0.93	8	$\sim10^{-9}$	0.22	0.10	−

[a] Defined as 1/e decay time for $<\delta V(t)\cdot\delta V(0)>$. [b] Determined from measured efficiency via eq 4.1. [c] Inverse of average rate constant for $^{5'}$A → 2AP and $^{3'}$A → 2AP.

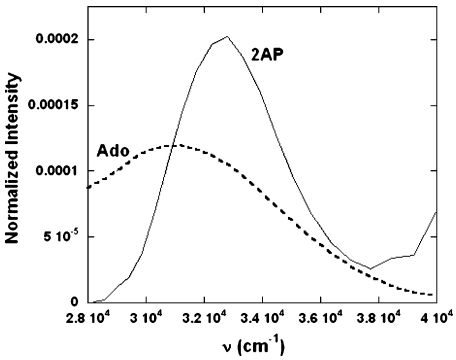

Figure 12. Normalized 2AP absorption spectrum ($\epsilon_{2AP}(\nu)/\nu$) and adenosine fluorescence spectrum ($\times a6_{ado}(\nu)/\nu^3$) for calculation of the spectral overlap term, as described in eq 3.8. The adenosine spectrum was taken from ref 61.

cies. It is possible that the MD simulations have failed to provide sufficient sampling of higher energy, unstacked configurations, inclusion of which would lead to a reduction in the ensemble-averaged rate; however, the good agreement between the simulated and experimental anisotropy data suggests this is not the case. A second possibility for the discrepancies between the calculated rates and the experimentally derived ones is the use of the spectral overlap procedure for determining the Franck−Condon contribution to the rate. This assumes the steady-state donor and acceptor spectral line shapes reflect relaxation processes that are faster than the transfer time. While the transfer time observed here (i.e. <1 ps) is somewhat slower than aqueous solvation dynamics, it is comparable to typical vibrational relaxation times for high frequency modes in molecules of this size; thus, the spectral line shapes may still be evolving on the time scale of EET between A and 2AP. It is possible that a model that partitions the spectral broadening into "slow" and "fast" components would yield a lower value for the nuclear contribution than does the homogeneous model described here; however, such a model would require new information on the excited state relaxation dynamics of the bases and would need to consider the possibility of temporal correlations in the energetic fluctuations of the donor and acceptor states. It is also conceivable that fluctuation-induced mixing of localized monomer states and charge-transfer states arising from orbital overlap terms not included in our model lead to non-negligible contributions to the rate in stacked conformations. Extension of the MD-TDC method to include this mixing is currently underway.

It is interesting to note that though the 2AP-labeled trinucleotides exhibit a high degree of conformational flexibility with significant fluctuations in the Coulombic coupling on the picosecond time scale, the fractional contribution to the rate from structural dynamics (shown in Table 2) is negligible. The reason for this is that the mean square value of the coupling is much greater than the variance in the coupling. This has been discussed by Balabin and Onuchic,[62] who defined a coherence parameter, $\langle V\rangle^2/\langle V^2\rangle$ (also shown in Table 2), for estimating the relative importance of dynamic fluctuations in determining the rate. For the case of energy transfer in the deoxytrinucleotides, this number is close to unity, indicating that the rates are governed by the mean square value of the coupling (i.e., slow fluctuation limit). This appears to be a qualitatively different situation than that encountered in 2AP photoinduced charge-transfer processes in these systems, where the temperature and viscosity dependence of the charge-transfer efficiencies suggest dynamic fluctuations in the electronic coupling are important. This has important implications for 2AP as a DNA structural probe. *While both energy transfer efficiencies and charge-transfer rates provide useful information on the extent of stacking of 2AP with its flanking bases, they do so on time scales that differ by nearly 3 orders of magnitude.*

Finally, we point out that both the ensemble-averaged TDC and dipole−dipole rates predict that transfer from the $^{5'}$A → 2AP transfer is measurably faster than the $^{3'}$A → 2AP transfer, in accord with the experimental results on the transfer efficiencies. It is evident that a simple interpretation of the transfer efficiency as a direct measure of the "extent" of stacking is problematic if one uses a structural metric such as the base−base center-of-mass distance.

5. Summary and Conclusions

The significance of this work is two-fold: First, the use of MD to sample the time scales of structural motions allows the effects of structural dynamics on the electronic coupling to be accounted for in a Förster-like expression for the transfer rate constant, which we have done here through the model of Troisi et al.[55] This is a largely unexplored region of the Förster theory.[63] The majority of users of Förster theory (e.g., FRET experimenters) assume that $\kappa^2 = 2/3$, which applies a single average value to a dynamically varying parameter. The most careful FRET work[64,65] still utilizes the assumption that the donor−acceptor orientations are uncorrelated with their separations—an assumption that is completely invalid in the current work. The presence of correlation between κ^2 and R_{DA} is likely to be found in the future as FRET is applied to more and more challenging systems, such as membrane proteins, protein−protein and protein−DNA complexes, and single molecules. By combining the MD sampling of structural fluctuations with the TDC method, this dynamic evaluation of the coupling is easily extended to systems with all but the smallest of donor−acceptor separations.

Second, using steady-state and time-resolved fluorescence anisotropy and molecular dynamics simulations, we have shown that the DNA trinucleotides $^{5'}$dTp2APpA$^{3'}$ and $^{5'}$dTp2APpA$^{3'}$ exist in solution largely as stacked structures but with a high degree of conformational flexibility. Application of the MD-TDC method to these systems shows that structural fluctuations significantly modulate the coupling between 2AP and its neighbors on the sub-100 picosecond time scale. Despite these rapid fluctuations in the electronic interaction, the mean square value of the coupling is sufficiently large that the rate of energy transfer is determined solely by the static properties of the ensemble. The measured transfer efficiencies thus reflect the

competition between the mean square coupling and the lifetime of the donor adenosine. Previous studies of fluorescence quenching in these systems following direct excitation of the 2AP $\pi-\pi^*$ state have shown that structural dynamics are important in determining the rate of 2AP → N charge transfer and, hence, the degree of quenching. Thus, although both energy transfer and charge transfer efficiencies provide sensitive probes of base stacking, they do so over vastly different time windows.

Acknowledgment. J.M.J. gratefully acknowledges the ACS Petroleum Research Fund for support of this work through Grant No. 36506-AC6, Ms. Jennifer Boots for the synthesis and purification of the DNA trinucleotides, and Dr. Scott A. Showalter and Dr. B. Macgregor for useful discussions. B.P.K. gratefully acknowledges support from the Research Corporation Cottrell College Science Awards, the ACS Petroleum Research Fund, and the Towsley Foundation. J.M.J. and B.P.K. together acknowledge support from the Pew Midstates Science and Mathematics Consortium.

References and Notes

(1) Brauns, E. B.; Madaras, M. L.; Coleman, R. S.; Murphy, C. J.; Berg, M. A. *J. Am. Chem. Soc.* **1999**, *121*, 11644.

(2) Brauns, E. B.; Berg, M. A. *Phys. Rev. Lett.* **2002**, *88*, 15801.

(3) Okonogi, T. M.; Reese, A. W.; Alley, S. C.; Hopkins, P. B.; Robinson, B. W. *Biophys. J.* **1999** *77*, 3256.

(4) Young, M. A.; Ravishanker, G.; Beveridge, D. L. *Biophys. J.* **1997**, *73*, 2313.

(5) Troisi, O.; Orlandi, G. *J. Phys. Chem. B.* **2002**, *106*, 2093.

(6) Nordlund, T. M.; Andersson, L.; Nilsson, L.; Rigler, R.; Gräslund, A.; McLaughlin, L. W. *Biochemistry* **1989**, *28*, 9095.

(7) Guest, C. R.; Hochstrasser, R. A.; Sowers, L. C.; Millar, D. P. *Biochemistry* **1991**, *30*, 3271.

(8) Bloom. L. B.; Otto, M. R.; Beechem, J. M.; Goodman. M. F. *Biochemistry* **1993**, *32* 11247.

(9) Jia, Y.; Kumar, A.; Patel, S. S.; *J. Biol. Chem.* **1996**, *271*, 30451.

(10) Ujvari, A.; Martin, C. T. *Biochemistry* **1996**, *35*, 14574.

(11) Stivers, J. T. *Nucleic Acids Res.* **1998**, *26*, 3837.

(12) Wilson, T. J.; Zhao, Z. Y.; Maxwell, K. Kontogiannis, L.; Lilley, D. M. *Biochemistry* **2001** *38*, 5317.

(13) Allan, B. W.; Reich, O.; Beechem, J. *Biochemistry* **2001**, *38*, 5308.

(14) Rachofsky, E. L.; Seibert, E.; Stivers, J. T.; Osman, R.; Ross, J. B. A. *Biochemistry* **2001**, *40*, 957.

(15) Larsen, O. F. A.; van Stokkum, I. H. M.; Gobets, B.; van Grondelle, R.; van Ameroengen, H. *Biophys. J.* **2001**, *81*, 1115.

(16) Rist, M. J.; Marino, J. P. *Curr. Org. Chem.y* **2002**, *6*, 775.

(17) Rai, P.; Cole, T. D.; Thompson, E.; Millar, D. P., Linn, S. *Nucleic Acids Res.* **2003**, *31*, 2323.

(18) Su, T. J.; Connolly, B. A.; Darlington C.; Mallin R.; Dryden D. T. F. *Nucleic Acids Res.* **2004** *32*, 2223.

(19) Hall, K. B.; Willams, D. J. *RNA* **2004**, *10*, 34.

(20) Shchyolkina, A. K.; Kaluznhy, D. N.; Borisova, O. F.; Hawkins, M. E.; Jernigan, R. L.; Jovin, T. M.; Arndt-Jovin, D. J.; Zhurkin, V. B. *Nucleic Acids Res.* **2004** *32*, 432.

(21) Johnson, N. P.; Baase, W. A.; von Hippel, P. H. *Proc. Natl. Acad. Sci U.S.A.* **2004** *101*, 3426.

(22) Nordlund, T. M.; Xu, D.; Evans, K. O. *Biochemistry* **1993**, *32*, 12090.

(23) Kelley, S. O.; Barton, J. K. *Science* **1999**, *283*, 375.

(24) Wan, C. Z.; Fiebig, T.; Schiemann, O.; Barton, J. K.; Zewail, A. H. *Proc. Natl. Acad. Sci. U.S.A.* **2000**, *97*, 14052.

(25) Jean, J. M.; Hall, K. B. *Proc. Natl. Acad. Sci. U.S.A.* **2001**, *98*, 37.

(26) Jean, J. M.; Hall, K. B. *Biochemistry* **2002**, *41*, 13152.

(27) Nordlund, T. M.; Xu, D.; Evans, K. O. *Biochemistry* **1993**, *32*, 12090.

(28) Xu, D.; Evan, K. O.; Nordlund, T. M. *Biochemistry* **1994**, *33*, 9592.

(29) Xu, D.; Nordlund, T. M. *Biophys. J.* **2000**, *78*, 1042.

(30) Davis, S. P.; Matsumura, M.; Williams, A.; Nordlund, T. M. *J. Fluoresc.* **2003**, *13*, 249.

(31) O'Neill, M. A.; Barton, J. K. *Proc. Natl. Acad. Sci. U.S.A.* **2002**, *99*, 16543.

(32) Crespo-Hernández, C. E.; Cohen, B.; Kohler, B. *Nature* **2005**, *436*, 1141.

(33) Förster, T. Delocalized excitation and excitation transfer. In *Modern Quantum Chemistry*; Sinanoglu, O., Ed.; Academic Press: New York, 1965; A4, p 321.

(34) Scholes, G. D.; Andrews, D. L. *J. Chem. Phys* **1997**, *107*, 5374.

(35) Jean, J. M.; Hall, K. B. *Biochemistry* **2004**, *43*, 10277.

(36) Norberg, J.; Nilsson, L. *J. Phys. Chem*. **1996**, *100*, 2550.

(37) Norberg, J.; Nilsson, L. *Acc. Chem. Res.* **2002**, *35*, 465.

(38) Krueger, B. P.; Scholes, G. D.; Fleming, G. R. *J. Phys. Chem. B.* **1998**, *102*, 5376.

(39) Scholes, G. D.; Harcourt, R. D.; Ghiggino, K. P. *J. Chem. Phys*. **1995**, *102*, 9574.

(40) We refer to M^{eg} as a transition density to be consistent with previous work, though note that the densities of eq 3.2 are multiplied by volume; thus, they should be more properly referred to as transition charge distributions.

(41) McWeeny, R. *Methods of Molecular Quantum Mechanics*, 2nd ed; Academic Press: London, 1992.

(42) Kong, J.; White, C. A.; Krylov, A. I.; Sherrill, C. D.; Adamson, R. D.; Furlani, T. R.; Lee, M. S.; Lee, A. M.; Gwaltney, S. R.; Adams, T. R.; Ochsenfeld, C.; Gilbert, A. T. B.; Kedziora, G. S.; Rassolov, V. A.; Maurice, D. R.; Nair, N.; Shao, Y.; Besley, N. A.; Maslen, P. E.; Dombroski, J. P.; Daschel, H.; Zhang, W.; Korambath, P. P.; Baker, J.; Byrd, E. F. C.; Van Voorhis, T.; Oumi, M. Hirata, S.; Hsu, C.-P.; Ishikawa, N.; Florian, J.; Warshel, A.; Johnson, B. G.; Gill, P. M. W.; Head-Gordon, M.; Pople, J. A. *J. Comput. Chem.* **2000**, *21*, 1532.

(43) Ortiz, W.; Krueger, B. P.; Kleiman, V. D.; Krause, J. L.; Roitberg, A. E. *J. Phys. Chem. B.* **2005**, *119*, 11512.

(44) Cornell, W. D.; Cieplak, P.; Bayly, C. I.; Gould, I. R.; Merz, K. M.; Ferguson, D. M.; Spellmeyer, D. C.; Fox, T.; Caldwell, J. W.; Kollmann, P. A. *J. Am. Chem. Soc.* **1995**, *117*, 5179.

(45) Case, D. A.; Pearlman, D. A.; Caldwell, J. W.; Cheatham, T. E., 3rd; Wang, J. M.; Ross, W. S.; Simmerling, C.; Darden, T.; Merz, K. M.; Stanton, R. V.; Cheng, A.; Vincent, J. J.; Crowley, M.; Tsui, V.; Gohlke, H.; Radmer, R.; Duan, Y.; Pitera, J.; Massova, I.; Seibel, G. L.; Singh, U. C.; Weiner, P.; Kollman, P. A. *AMBER 7*; University of California: San Francisco, CA, 2002.

(46) Beveridge, D. L.; Barreiro, G.; Byun, K. S.; Case, D. A.; Cheatham, T. E., III; Dixit, S. B.; Giudice, E.; Lankas, F.; Lavery, R.; Maddocks, J. H.; Osman, R.; Seibert, E.; Sklenar, H.; Stoll, G.; Thayer, K. M.; Varnai, P.; Young, M. A. *Biophys. J.* **2004**, *87*, 3799.

(47) Arthanari, H.; McConnell, K. J.; Beger, R.; Young, M. A.; Beveridge, D. L.; Bolton, P. H. *Biopolymers* **2003**, *68*, 3.

(48) Bevan, D. R.; Li, L.; Pedersen, L. G.; Darden, T. A. *Biophys. J.* **2000** *78*, 668.

(49) Orozco, M.; Perez, A.; Noy, A.; Luque, F. J. *Chem. Soc. Rev.* **2003**, *32*, 350.

(50) MacKerrell, A. D., Jr. *J. Comput. Chem.* **2004**, *25*, 1584.

(51) Giudice, E.; Lavery, R. *Acc. Chem. Res.* **2002**, *35*, 350.

(52) TDDFT calculations (B3LYP/6-311+G(d,p)) predict $S_0 \rightarrow S_2$ is the lowest energy $n-\pi^*$ transition (unpublished result).

(53) ONeill, M. A.; Becker, H.-C.; Wan, C.; Barton, J. K.; Zewail, A. H. *Angew. Chem., Int. Ed*. **2003**, *42*, 5896.

(54) O'Neill, M. A.; Dohno, C.; Barton, J. K. *J. Am. Chem. Soc.* **2004** *126*, 1316.

(55) Troisi, A.; Nitzan, A.; Ratner, M. A. *J. Chem. Phys.* **2003**, *119*, 5782−5788.

(56) Pecourt, J.-M. L.; Peon, J.; Kohler, B. *J. Am. Chem. Soc*. **2000**, *100*, 3943.

(57) Holmén, A.; Nordén, B.; Albinsson, B. *J. Am. Chem. Soc*. **1997**, *119*, 3114−3121.

(58) Holmén, A.; Broo, A.; Albinsson, B Nordén, B. *J. Am. Chem. Soc*. **1997**, *119*, 12240.

(59) Callis, P. R. *Annu. Rev. Phys. Chem*. **1983**, *34*, 329.

(60) Lipari, G.; Szabo, A. *Biophys. J.* **1980**, *30*, 489−506.

(61) Andréasson, J.; Holmén, A.; Albinsson, B. *J. Phys. Chem. B* **1999**, *103*, 9782.

(62) Balabin, I. A.; Onuchic, J. N. Science **2000**, *290*, 114.

(63) Clegg, R. M. In *Fluorescence Imaging and Microscopy*; Wang, X. F., Herman, B., Eds.; John Wiley & Sons: New York, 1996; pp 179−252.

(64) Dale, R. E.; Eisinger, J.; Blumberg, W. E. *Biophys. J.* **1974**, *26*, 161.

(65) Dale, R. E.; Eisinger, J. *Biopolymers* **1974**, *13*, 1573.